AMERICAN SOCIETY FOR MICROBIOLOGY | mBio®

RESEARCH ARTICLE

The Atomic Structure of the Phage Tuc2009 Baseplate Tripod Suggests that Host Recognition Involves Two Different Carbohydrate Binding Modules

Pierre Legrand,[a] Barry Collins,[d] Stéphanie Blangy,[b,c] James Murphy,[d] Silvia Spinelli,[b,c] Carlos Gutierrez,[e] Nicolas Richet,[a] Christine Kellenberger,[b,c] Aline Desmyter,[b,c] Jennifer Mahony,[d] Douwe van Sinderen,[d,f] Christian Cambillau[b,c]

Synchrotron Soleil, L'Orme des Merisiers, Gif-sur-Yvette Cedex, France[a]; Architecture et Fonction des Macromolécules Biologiques, Aix-Marseille Université, Campus de Luminy, Marseille, France[b]; Architecture et Fonction des Macromolécules Biologiques, Centre National de la Recherche Scientifique (CNRS), Campus de Luminy, Marseille, France[c]; School of Microbiology, University College Cork, Cork, Ireland[d]; Research Institute of Biomedical and Health Sciences, Universidad de Las Palmas de Gran Canaria (ULPGC), Las Palmas, Canary Islands, Spain[e]; APC Microbiome Institute, University College Cork, Cork, Ireland[f]

ABSTRACT **The Gram-positive bacterium *Lactococcus lactis*, used for the production of cheeses and other fermented dairy products, falls victim frequently to fortuitous infection by tailed phages. The accompanying risk of dairy fermentation failures in industrial facilities has prompted in-depth investigations of these phages. Lactococcal phage Tuc2009 possesses extensive genomic homology to phage TP901-1. However, striking differences in the baseplate-encoding genes stimulated our interest in solving the structure of this host's adhesion device. We report here the X-ray structures of phage Tuc2009 receptor binding protein (RBP) and of a "tripod" assembly of three baseplate components, BppU, BppA, and BppL (the RBP). These structures made it possible to generate a realistic atomic model of the complete Tuc2009 baseplate that consists of an 84-protein complex: 18 BppU, 12 BppA, and 54 BppL proteins. The RBP head domain possesses a different fold than those of phages p2, TP901-1, and 1358, while the so-called "stem" and "neck" domains share structural features with their equivalents in phage TP901-1. The BppA module interacts strongly with the BppU N-terminal domain. Unlike other characterized lactococcal phages, Tuc2009 baseplate harbors two different carbohydrate recognition sites: one in the bona fide RBP head domain and the other in BppA. These findings represent a major step forward in deciphering the molecular mechanism by which Tuc2009 recognizes its saccharidic receptor(s) on its host.**

IMPORTANCE **Understanding how siphophages infect *Lactococcus lactis* is of commercial importance as they cause milk fermentation failures in the dairy industry. In addition, such knowledge is crucial in a general sense in order to understand how viruses recognize their host through protein-glycan interactions. We report here the lactococcal phage Tuc2009 receptor binding protein (RBP) structure as well as that of its baseplate. The RBP head domain has a different fold than those of phages p2, TP901-1, and 1358, while the so-called "stem" and "neck" share the fold characteristics also found in the equivalent baseplate proteins of phage TP901-1. The baseplate structure contains, in contrast to other characterized lactococcal phages, two different carbohydrate binding modules that may bind different motifs of the host's surface polysaccharide.**

Received 15 October 2015 **Accepted** 21 December 2015 **Published** 26 January 2016

Citation Legrand P, Collins B, Blangy S, Murphy J, Spinelli S, Gutierrez C, Richet N, Kellenberger C, Desmyter A, Mahony J, van Sinderen D, Cambillau C. 2016. The atomic structure of the phage Tuc2009 baseplate tripod suggests that host recognition involves two different carbohydrate binding modules. mBio 7(1):e01781-15. doi:10.1128/mBio.01781-15.

Invited Editor Venigalla Rao, Catholic University of America **Editor** Michael G. Rossmann, Purdue University

Address correspondence to Douwe van Sinderen, d.vansinderen@ucc.ie, or Christian Cambillau, cambillau@afmb.univ-mrs.fr.

Most viruses that infect bacteria—commonly termed bacteriophages (or phages)—belong to the *Caudovirales* order: they possess a tail for host recognition, adhesion, and genome delivery—three steps essential for host infection. Phages typically employ adhesion modules that are located on the capsid, tail tube, and/or tail tip to facilitate host scanning and reversible attachment to cell-wall-associated saccharides (1–6), as recently evidenced (7, 8). Following this reversible attachment, host-specific and irreversible adhesion is the exclusive responsibility of proteins located on the tail tip (9, 10). In *Myoviridae*, genome injection follows contraction of its long tail, thus leading to host cell piercing (11–13), while in *Podoviridae* (phages with short tails) and *Siphoviridae* (phages with long noncontractile tails), other mechanisms of nucleic acid delivery are presumed to occur (6, 8, 11).

Phages recognize and bind either a membrane protein receptor or a carbohydrate moiety located in or on the cell envelope of a specific host (6, 14, 15). Examples of bacteriophages that recognize proteinaceous receptors are the coliphages lambda and T5, which recognize LamB and FhuA, respectively, both located on the surface of the *Escherichia coli* cell envelope (16–19), and *Bacillus* phage SPP1 or lactococcal phage c2, which recognize the YueB or PIP membrane proteins emerging at the host's cell surface (20, 21). The tail tip of phages that recognize a membrane protein receptor exhibits an elongated morphology as it extends out of the

distal tail end as a fiber (6). In contrast, characterized myo- or siphophages that employ carbohydrate-dependent host recognition possess a large heteropolymeric proteinaceous organelle, also called the baseplate, with a multitude of individual binding sites to ensure efficient and specific host adsorption (22–25). In the case of myophage T4, host binding follows a two-step mechanism whereby the baseplate-associated long tail fibers first reversibly bind lipopolysaccharide (LPS) or OmpC (26–29), causing a conformational change in the baseplate that then allows irreversible binding of the short tail fibers to LPS (30).

Siphophage baseplates have been thoroughly investigated in the case of the Gram-positive bacterium *Lactococcus lactis*. *L. lactis* is commonly employed as a starter culture in various dairy fermentation processes, and its intensive industrial exploitation has facilitated the isolation of a very large number of phages infecting various strains of this bacterium (31, 32). Lactococcal phages have been grouped into 10 different species based on DNA homology and morphology (33). Among these, representatives of the P335 and 936 species are the most commonly encountered phages in the dairy environment, and their characterized members possess a baseplate and thus are thought to recognize and bind to a cell-wall-associated saccharidic receptor (34). A striking feature of lactococcal phages, in particular the 936 and P335 species, is their extraordinary abundance and specificity: each phage infects just a single or very small number of hosts with exquisite specificity among hundreds of different *L. lactis* strains (35–37). An extracellular phospho-polysaccharide (the so-called "pellicle") was shown to be required for infection of *L. lactis* MG1363 by phage p2, a member of the 936 species (38). Different pellicle polysaccharides have been identified for *L. lactis* strains 3107 and SMQ-388, and these were shown to serve as receptors of phage TP901-1 (the P335 species) (39) and phage 1358 (the 1358 species) (40). The diverse combination of monosaccharide moieties within a penta/hexasaccharidic motif is likely responsible for the particular host specificity of individual lactococcal phages.

In order to understand the molecular mechanism of lactococcal phage-host recognition, we determined the atomic structures of the receptor binding proteins (RBPs) of four representatives of three lactococcal phage species, belonging to the most abundant species: 936 (two representatives, phages p2 and bIL170) (41), P335 (phage TP901-1) (24, 42), and 1358 (phage 1358) (40). We also determined the crystal structures of the baseplates of phage p2 (23) and phage TP901-1 (25), revealing striking differences between their host recognition mechanisms (22, 23, 25, 43). The baseplate of p2 (936 species) undergoes a dramatic, Ca^{2+}-dependent conformational change as a prerequisite for host infection (10, 23, 44). In contrast, the baseplate of TP901-1 (P335 species) is maintained in a structural configuration that is Ca^{2+} independent and "ready to use" (25, 45). In the case of TP901-1, each of the six receptor-binding subunits, or so-called tripods that are suspended from the hexameric Dit protein of the baseplate, is composed of three BppU and nine BppL protein monomers (25).

Lactococcal phage Tuc2009 (P335 species) is a close relative of phage TP901-1, although they infect different hosts: *L. lactis* UC509.9 (or SMQ380) and 3107 (or SMQ415), respectively (39, 46). The Tuc2009 RBP and baseplate components have previously been expressed as soluble modules, making it possible to obtain a low-resolution "in solution" model (47), followed by the determination of the low-resolution structures of the virion's baseplate and of the expressed tripod (composed of a BppUct/BppA/BppL heteropolymer [see below]) by negative-staining electron microscopy (48). Tuc2009 structural proteins share 95 to 99% sequence identity with those of TP901-1, with the exception of the RBP (also called BppL). Furthermore, the C terminus of Tuc2009-encoded BppU contains a 25-residue extension (BppUct), and the baseplate contains an accessory protein, BppA, whose precise role in adsorption has remained elusive (48). Despite the availability of soluble proteins and its similarity to equivalent TP901-1 proteins, the Tuc2009 RBP and the "tripod" have stubbornly resisted exhaustive crystallization attempts.

In this report, we employed a combination of limited proteolysis and the use of so-called "nanobodies" (49) to crystallize Tuc2009 RBP and determined its structure, together with that of the "tripod," making it possible to determine the overall structure of the Tuc2009 baseplate. The atomic structures demonstrate that the RBP domain involved in host recognition (the so-called "head") of Tuc2009, although a β-domain, exhibits a fold different from that of its TP901-1 equivalent. Surprisingly, we discovered that BppA possesses a carbohydrate binding domain with an extended saccharidic binding site, suggesting that this protein participates in receptor binding together with the bona fide RBP.

RESULTS

The nanobody L06 structure. Despite extensive and exhaustive efforts, all of our attempts to crystallize Tuc2009 RBP (open reading frame 53 [ORF53] or BppL) had been unsuccessful. We therefore decided to immunize a camel with this protein, hoping that generation of and subsequent association with specific nanobodies would promote crystallization, as had previously been observed (49), while it was also hoped that it would render effective neutralizers of phage infection. Following an established procedure (described in reference 49), we isolated nano-L06 that could be expressed at reasonable yields (5 mg/liter). Nano-L06 crystallized readily, and a data set was collected at 1.1-Å resolution at Soleil Proxima 1 (Table 1). Nano-06 exhibits the classical 9-stranded β-sandwich fold of nanobodies with a long CDR3 frequently observed in nanobodies from dromedaries, in contrast with those originating from llamas (Fig. 1). The 17-residue-long CDR3 forms a long loop followed by a 2.5 turn α-helix. A disulfide bridge is observed between the CDR3 Cys 100h and the framework Cys 45.

The nanobody L06/RBP complex structure. We cocrystallized the RBP with nano-L06, although the RBP had unfortunately been cleaved by trypsin digestion prior to complex purification. A data set was collected at a 2.70-Å resolution at beamline Soleil Proxima 1 (Table 1), and the corresponding structure of the cocrystallized complex was solved by molecular replacement using the obtained nano-L06 structure (described above). The complex contains a trimeric RBP domain and three nano-L06 moieties (Fig. 2A and B). The N-terminal part of the RBP is not visible in the electron density map, as the model could be built from residue Asp 47 to residue Asn 173 (Fig. 2A to C).

The RBP structure starts with a 12-residue-long N-terminal α-helix (residues 49 to 61) followed by a 12-strand β-barrel, constituting the so-called "head" domain (Fig. 2C and D). At the "bottom" of the RBP head monomer, a first antiparallel β-sheet assembles β1-β12-β3-β8-β6 and stacks against strands β2-β9 (Fig. 2D). At the "top" of the domain, strands β11-β4 face the β7-β5-β10 β-sheet (Fig. 2C and D).

Each nanobody interacts with two RBP monomers (see Ta-

TABLE 1 Data collection and refinement statistics

Parameter	Result for[a]: Nano-L06 (S-SAD)	Nano-L06	RBP/nano-L06	Tripod
Data collection				
PDB no.		5E7B	5E7F	5E7T
Source	Soleil PX 1	Soleil PX 1	Soleil PX 1	Soleil PX 1
Wavelength (Å)	1.7712	0.8856	0.9786	1.0087
Space group	$P6_522$	$P6_522$	$P2_12_12_1$	$P2_13$
Cell dimension (Å)	$a = b = 52.1, c = 162.7$	$a = b = 52.1, c = 162.7$	$a = 84.7, b = 88.0, c = 147.6$	$a = b = c = 212.0$
Angles (°)	$\alpha = \beta = 90, \gamma = 120$	$\alpha = \beta = 90, \gamma = 120$	$\alpha = \beta = \gamma = 90$	$\alpha = \beta = \gamma = 90$
Resolution limits (Å)	45.1–1.9 (2.01–1.9)	45.1–1.1 (1.13–1.1)	47.1–2.7 (2.77–2.7)	34.9–2.9 (3.0–2.9)
R_{merge}	0.055 (0.086)	0.068 (1.55)	0.146 (1.60)	0.187 (1.91)
$CC_{1/2}$	100 (99.7)	100 (61.7)	99.7 (74.8)	99.7 (50.6)
No. of unique reflections	16,724 (561)	52,014 (3,596)	31,023 (2,264)	70,164 (6,732)
Mean $I/\sigma\langle I\rangle$	61.92 (20.74)	18.4 (1.5)	11.0 (1.2)	10.7 (1.25)
Completeness (%)	85.9 (39.1)	96.6 (91.7)	99.9 (99.9)	99.8 (99.3)
Multiplicity	37.2 (14.6)	19.5 (19.2)	7.2 (7.1)	13.7 (13.7)
SigAno	1.534 (0.841)			
CC_{ano} CC_{all}/CC_{weak}	37.6/22.2			
FOM	0.4			
Refinement				
Resolution (Å)		15.0–1.10 (1.1125–1.10)	34.5–2.7 (2.79–2.7)	34.9–2.9 (2.98–2.9)
No. of reflections		51,977 (2,905)	31,009 (2,812)	70,164 (5,103)
No. of protein/water/ligand atoms		1,968/188	5,848/40	8,126/61/47
No. of test set reflections		2,359	1,550	3,508
R_{work}/R_{free} (%)		15.8/18.9 (31.6/30.6)	19.4/20.8 (28.0/35.6)	21.4/23.7 (28.2/31.7)
RMSD bonds (Å)/angles (°)		0.0096/1.37	0.008/1.02	0.01/1.18
B Wilson/B avg		14.3/23.0	75.1/78.7	104.0/104.5
Ramachandran preferred/allowed/outliers (%)		98.6/1.4/0	98.0/2.0/0	95.1/4.8/0.1

[a] Numbers in parentheses refer to the highest-resolution bin.

ble S1 in the supplemental material). It is noteworthy that the interactions reported by the PISA server (50) are quite different at the three interfaces, as the buried surface area (BSA) values of the nanobodies are 638, 609, and 840 Å^2 for monomers A, B, and C, respectively. Similarly, the BSA values for RBP monomers G, H, and I are 764, 636, and 787 Å^2 (see Table S1). The interaction

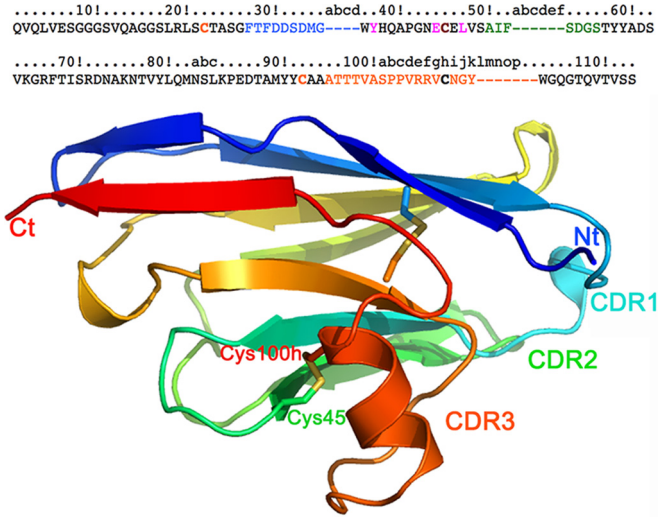

FIG 1 Sequence and structure of nanobody nano-L06. The sequence (above) is given following the Khabat numbering. CDR1 to -3 are colored blue, green, and orange, respectively. The ribbon structure (below) is rainbow colored with the CDRs in blue, green, and orange. The extra disulfide bridge between Cys 45 and Cys 100h is indicated. Ct, C terminal; Nt, N terminal.

involves the three CDRs but is dominated by CDR3 (see Table S1). On the RBP, most of the contacts of the first nanobody are established with the N-terminal helix (638 Å^2), and the remaining interactions involve loops 68 to 71 (185 Å^2), while the second nanobody interacts with loops 113 to 116 (147 Å^2) and 139 to 142 (45 Å^2), all of these loops being localized at the RBP "bottom." A DALI server (51) search retrieved several significant hits: the best reported hit was a virulence plasmid protein pgp3-d (4JDO, Z = 8.1, root mean square deviation [RMSD] = 2.6 Å on 100 residues), and the second was a lectin, the N-terminal domain of bc2l-c lectin from *Burkholderia cenocepacia* (52) (2WQ4, Z = 7.9, RMSD = 2.7 Å on 95 residues). It is noteworthy that these domains bear no fold similarity to the head domains of other structurally characterized lactoccocal phage RBPs—i.e., those of phages p2, TP901-1, and 1358 (40, 42, 53).

The Tuc2009 tripod structure. Following a strategy similar to that employed for the baseplate structure of phage TP901-1 (25, 54), we expressed the so-called "tripod" of Tuc2009 (48). In TP901-1, the tripod is an assembly of a trimer of BppU (involving the 100 C-terminal residues of BppU) and three trimers of BppL (25). The situation is more complex with Tuc2009: we know from negatively stained electron microscopy (EM) images that such a tripod can be observed (48) and that it comprises the 100 C-terminal residues of BppU, followed by a C-terminal extension of ~25 residues specific to Tuc2009 and implicated in BppA association, the supplementary BppA protein, and BppL. This complex (in association with nano-L06) was crystallized, and a data set was collected at a 2.9-Å resolution at Soleil Proxima 1 (Table 1).

The tripod structure was solved by molecular replacement using similar, previously determined structures: the trimeric struc-

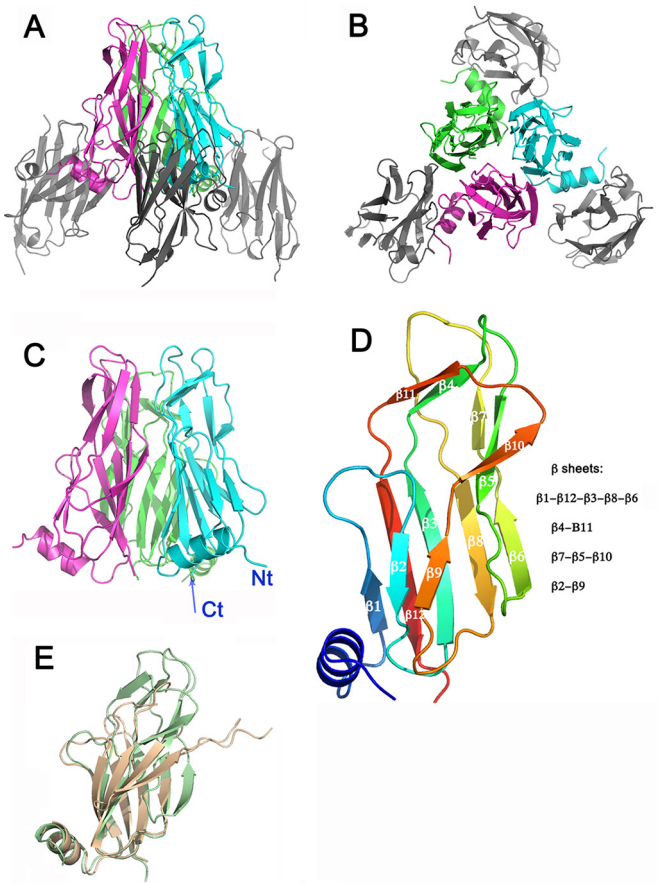

FIG 2 Structure of the RBP head domain in complex with nano-L06. (A) Ribbon view of the RBP head domain trimer (monomers colored blue, green, and pink) bound to three nano-L06 proteins (colored gray). (B) Ninety degree rotated view. Note the contact of nano-L06 with the helix of one monomer and the loops of a second one. (C) Ribbon view of the RBP head domain trimer (monomers colored blue, green, and pink). (D) Ribbon view of the RBP head domain monomer (rainbow colored) with the β-strands numbered β1 to β12. (E) Superposition between RBP monomers from the nano-L06/RBP complex (green) and the serendipitous domain found in the tripod structure (beige). The RMSD value is 2.4 Å.

ture of the Tuc2009 RBP head domain described above (residues 61 to 173) and the 100 C-terminal residues of BppU from TP901-1 that exhibit ~95% identity with the corresponding part of Tuc2009 BppU. These two elements were localized easily with Molrep (55) or Phaser (56) and provided interpretable initial electron density maps. We then built the rest of the complex using alternated cycles of model building, solvent flattening, and refinement (see Materials and Methods). We completed the initial model by building the BppL stem region (residues 1 to 60), the BppU C-terminal extension (BppUct [residues 294 to 322]), and the complete BppA. A large additional density could account for a serendipitous extra monomer of the RBP head, with a conformation significantly different compared to the one in the head/nano-L06 complex and that of the tripod/nano-L06 complex. The asymmetric unit contains 1/3 tripod (Fig. 3A), the complete tripod sitting on the crystallographic 3-fold axis. Hence, the complete tripod complex is composed of 3 BppUct, 3 BppA, and 3 RBP trimers (Fig. 3B and C), which is consistent with observations using Wyatt analysis (48). Since the negatively stained EM map was available from a previous study, we used Chimera (57) to fit the complete tripod into the EM map (emd_2343.map at EMDB). The observed fit (ml = 0.83; 2,855/20,952 atoms outside contour) is good for the central part of the tripod, BppUct and BppL, but is not satisfactory for BppA (Fig. 3D). It is clear that BppA in the X-ray structure is rotated toward the tripod bottom (direction of RBP head), while it is situated higher in the EM map. However, the BppA volume of the X-ray structure is compatible with that of the EM map.

The trimeric RBP chain could be identified in the electron density map from Ala 2 to Asn 173 (Fig. 3A). The N-terminal segment of the RBP or so-called "stem" domain (residues 2 to 28) closely resembles that of TP901-1 as it starts with an elongated stretch (residues 2 to 10) followed by a turn and an α-helix (12–27) (Fig. 3A). An interlaced triple β-helix encompasses residues 29 to 59. This is followed by a loosely packed segment (residues 58 to 62) joining the triple β-helix to the head domain. However, the head domain, between residues 63 and 173, exhibits a very weak electron density map and consequently elicits very high B-factors. Noteworthy and surprisingly, a part of the triple β-helix and of the junction segment (residues 49 to 61) was found in an α-helical conformation in the cleaved RBP/head/nano-L06 complex (Fig. 2C and D).

The RBP three N-terminal stem stretches of residues 10 to 15 form a cup that harbors a loop of BppU (residues 217 to 235), ensuring a stable association between BppU and the RBP in a manner identical to that observed for the corresponding components of phage TP901-1 (25) (Fig. 3A). The BppU domain from Pro 195 (the N terminus of the construct) to Val 295 is quasi-identical to its corresponding domain in TP901-1. In Tuc2009, however, it is followed by a 25-residue extension (residues 296 to 321) forming a β-hairpin (Fig. 3A and F). This hairpin interacts strongly with the C-terminal domain of BppA since it completes one of its β-sheets.

BppA can be traced from Ala 3 to Lys 286: it begins with a loosely structured segment (residues 3 to 29) followed by a compact domain (domain 1, residues 30 to 185) and a junction segment (residues 186 to 229) interacting with the N-terminal segment, and it terminates in a β-sandwich fold (domain 2, residues 230 to 286) harboring the extension that links it to BppU as mentioned above (Fig. 3A and F). A DALI server-mediated search for domain similarity was performed for BppA domain 1, which retrieved similarity to carbohydrate binding domains 1GUI (Z = 10.1, RMSD = 2.6 Å on 120 residues, [58]) and 1GU3 (Z = 10.1, RMSD = 2.7 Å on 121 residues [58]), with a polysaccharide occupying an extended crevice (Fig. 3E). We performed a similar search for BppA domain 2, to which the β-hairpin extension of BppU (residues 296 to 321) was added. This composite domain was found to be very similar to a titin domain, 2NZI (Z = 5.9, RMSD = 1 Å on 56 residues [59]) (Fig. 3F).

The serendipitously cleaved BppL head domain (residues 52 to 173) is docked against BppA domain 1 (Fig. 3A). A monomer is observed in the crystallographic asymmetric unit, and the trimer is reconstituted by the crystallographic 3-fold axis. It exhibits an N-terminal α-helix followed by the β-domain of the RBP head as observed in the cleaved RBP/head/nano-L06 complex, but with a significant conformational change of some β-strand traces, with an RMSD value of 2.4 Å, while the RMSD value between the RBP head domains in the tripod and in the nano-L06 complex is 0.4 Å. In fact, the upper part of the RBP comprising the short upper

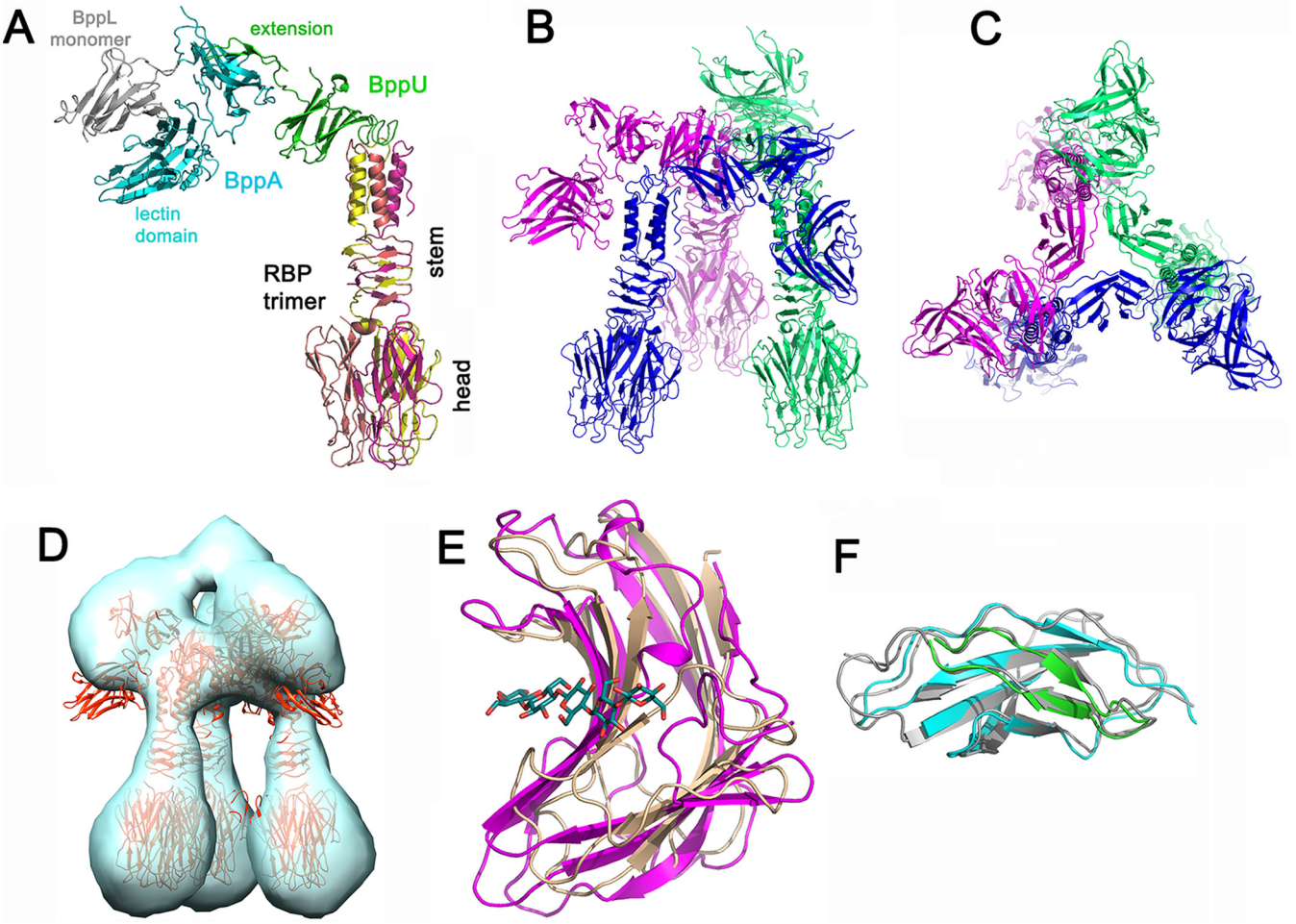

FIG 3 Structure of the Tuc2009 tripod and its domains. (A) Ribbon view of the tripod single unit assembling the RBP trimer (yellow, salmon, and pink), BppUct (green), BppA (blue), and a serendipitous RBP monomer (gray). (B) Ribbon view of the complete tripod reconstituted with the crystallographically single units. (The tripod sits on the cubic 3-fold axis.) The serendipitous RBP monomer has been omitted. (C) Ninety degree rotated view. (D) The tripod structure docked into the negatively stained EM map at a 23-Å resolution. (E) BppA domain 1 is superimposed onto the CBP structure of PDB entry 1GUI. The polysaccharide is from 1GUI. (F) BppA domain 2 is superimposed onto the titin domain of PDB entry 2NZI.

β-strands (as seen in Fig. 2C) has changed conformation, while the bottom part remained similar (Fig. 2E).

The Tuc2009 baseplate model. Knowing the atomic structure of Tuc2009 tripod facilitated the construction of a model of the complete baseplate of this phage based on the TP901-1 baseplate structure, since the Dit, Tal, and BppU C-terminal domains of the Tuc2009 baseplate are 99% identical to those of TP901-1. To build the Tuc2009 baseplate model, the BppU C-terminal domain of the TP901-1 baseplate was used to fit the Tuc2009 tripod onto the TP901-1 BppU/Dit complex. As demonstrated in our previous study, one of the BppA molecules (i.e., the most internal one) has to be removed from the tripod as it clashes with full-length BppU (48). Therefore, the Tuc2009 baseplate model assembles 93 proteins: those already found in TP901-1 baseplate, 6 Dit, 18 BppU, 54 BppL, and 3 Tal proteins (not included in the model), plus the 12 BppA proteins specific to Tuc2009 (Fig. 4A and B). This Tuc2009 baseplate model has a significantly larger diameter than that of TP901-1 (~320 Å versus ~270 Å) due to the BppA position at the baseplate periphery. We then superimposed the thus-obtained baseplate model on the low-resolution (34-Å) model based on a negatively stained EM map (emd-2340 at EMDB). We fitted it in the map using Chimera, which reported that 33,190 out of 154,323 (20%) atoms were situated outside the map (Fig. 4C). This rather mediocre result is due to the fact that the BppA molecules in the atomic structure are placed at a good radial position but are at a much lower position in the EM map. Most of the carbohydrate binding module (CBM) domain is therefore outside the map, thus explaining the poor fitting statistics. However, the remainder of the baseplate proteins (i.e., the Dit, BppU, and BppL subunits) all fit very well in the EM map (10% of atoms outside boundaries). The apparently lower position of BppA may be explained by the fact that BppA is joined to the baseplate core by a flexible linker and that the position of BppA may consequently be influenced by its surroundings, being different in the tripod compared to the virion's baseplate, or by differences generated by the two techniques employed (EM versus X-ray). This flexibility is likely to have functional implications in allowing improved accessibility to cell wall polysaccharides.

The putative saccharide binding site of RBP and BppA. We have seen that the RBP head domain has a fold similar to that of a

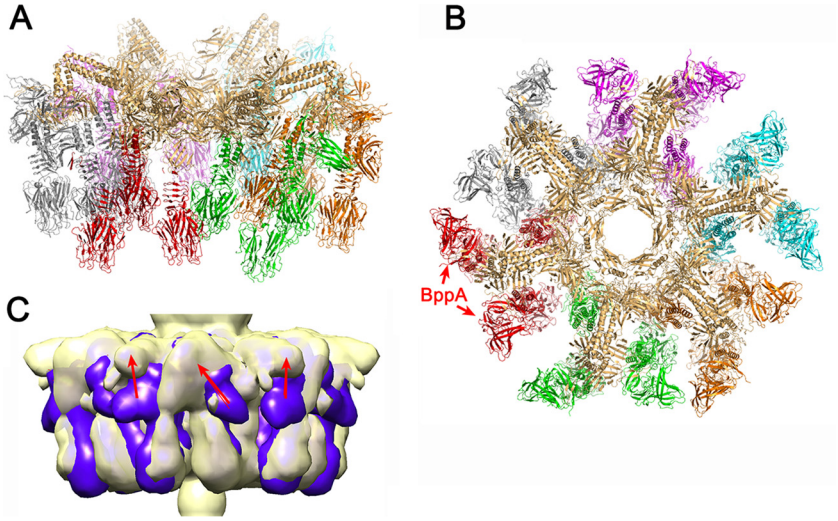

FIG 4 Structure of the Tuc2009 baseplate. (A) Ribbon view of the baseplate tilted by 30°. (B) Ribbon top view of the baseplate. The Dit and BppU proteins are colored beige; the RBPs have the same color within a tripod. (C) Superposition of the EM map of the baseplate (yellow) and of the baseplate map calculated at a 25-Å resolution, indicating the different positions of BppA at the periphery (red arrows).

trimeric lectin domain (2WQ4). The galactopyranoside Se derivative of the 2WQA structure binds in a crevice between two monomers in a typical saccharide binding site formed by an aromatic component (Tyr 48) and a strong network of hydrogen bonds involving Arg 85 and Arg 111, the carbonyl moiety of Thr 83, and the hydroxyl moiety of Thr 74. When positioned in Tuc2009 RBP, a typical saccharide binding is also observed involving Tyr 121, and hydrogen bond donors/acceptors Lys 162, His 163, Glu 101, and Asn 123 (Fig. 5) (data not shown). It is noteworthy that the saccharide binding site of phages TP901-1 and p2 is also located in a crevice between two monomers.

BppA was found to be similar to CBMs 1GUI and 1GU3. In the former structure, the bound saccharide exhibits a V-shape, while it is linear in the latter. When superimposing 1GUI and 1GU3 onto BppA-CBM (Fig. 5A), it is clear that the nature of the putative BppA-CBM saccharide binding site is not compatible with that of 1GU3. In contrast, it is very similar to the saccharide binding site of 1GUI—in both cases involving three tryptophan residues and several hydrogen bond donors/acceptors (Fig. 5B).

Nanobody binding and neutralization studies. We assayed the binding of nano-L06 to RBP and the tripod using biolayer interferometry (BLI). The nano-L06 was attached to the chip, and the RBP and tripod were dispensed over it at increasing concentrations (Fig. 6). A curve fitting using a 2:1 model (bivalent analyte) gave a K_d (dissociation constant) value of 9.1 ± 0.7 nM ($k_{on}{}^1 = 6.25 \times 10^4\ M^{-1}\ s^{-1}$, $k_{on}{}^2 = 27\ M^{-1}\ s^{-1}$, $k_{off}{}^1 = 5.77 \times 10^{-4}$, and $k_{off}{}^2 = 4.3\ s^{-1}$). The binding data of the tripod were analyzed using two methods. A curve fitting using a 2:1 model gave a K_d value of 9.1 ± 0.6 nM ($k_{on}{}^1 = 4.7 \times 10^4$ to $5.1 \times 10^4\ M^{-1}\ s^{-1}$, $k_{on}{}^2 = 34$ to $39\ M^{-1}\ s^{-1}$, $k_{off}{}^1 = 2.7 \times 10^{-4}$ to 2.8×10^{-4}, and

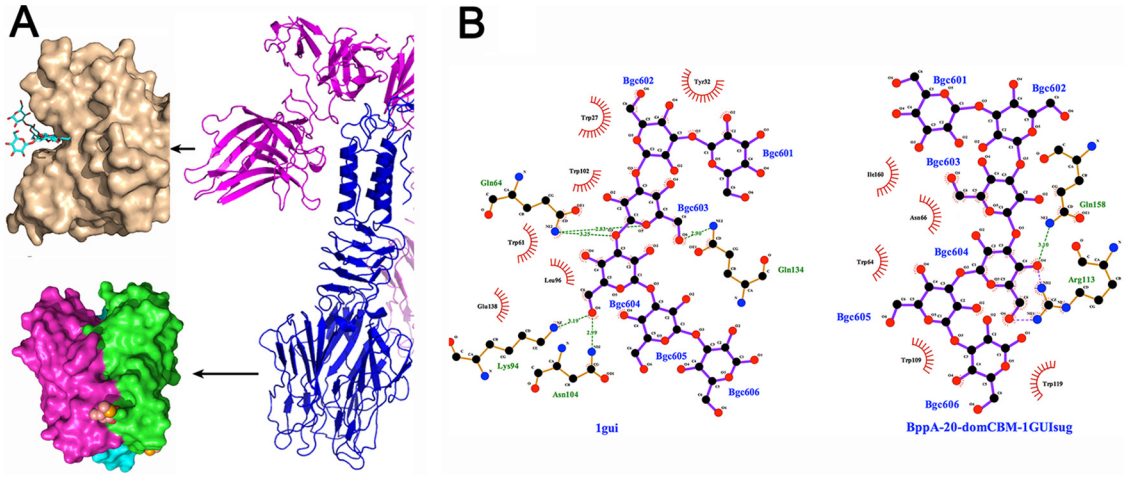

FIG 5 The Tuc2009 tripod domains and their putative saccharide binding sites. (A) Right, fragment of the Tuc2009 ribbon structure showing BppA and RBP domains. Left top, the BppA domain 1 and the polysaccharide from the related structure of the CBD in the PDB entry 1GUI. Left below, the RBP head domain and the saccharide from the related structure of the lectin in PDB entry 2WQ4. (B) The polysaccharide/protein contacts in the 1GUI PDB entry structure (left) and in the BPPA domain 1 in which the saccharide from 1GUI has been modeled.

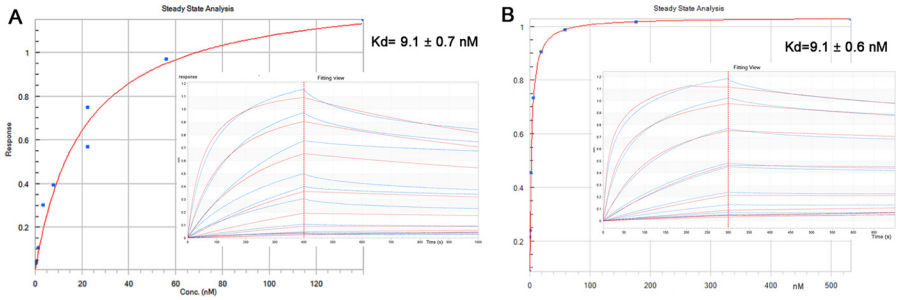

FIG 6 Biolayer interferometry (BLI). Shown are the results of binding data analysis using the steady-state method and curve fitting of the association and dissociation responses (insets). (A) Binding of Tuc2009 RBP to nanobody nano-L06 immobilized on the sensor chip and analyzed at steady state. (Inset) BLI recordings representing the binding and release of the RBP (from 1 to 140 nM). The variation of the response (shown as the experimental [red] and fitting curves [blue]) is reported on the *y* axis plotted versus the reaction time on the *x* axis (in seconds). (B) Binding of Tuc2009 tripod to nanobody nano-L06 immobilized on the sensor chip and analyzed at steady state. (Inset) BLI recordings representing the binding and release of the tripod (from 1 to 540 nM). The variation of the response (shown as the experimental [red] and fitting curves [blue]) is reported on the *y* axis plotted versus the reaction time on the *x* axis (in seconds).

k_{off}^2 = 1.94 to 3.7 s^{-1}), with satisfactory statistics. The improvement of the fitting upon using a 2:1 model reveals that besides the low-affinity site, nonspecific weak binding may also occur.

In order to discern if nano-L06 interfered with the infectious capability of Tuc2009, infection neutralization assays were performed (see Materials and Methods). This nanobody was not observed to inhibit infection of the lactococcal host strain UC509.9. This result was not completely unexpected for nano-L06 since the crystal structure revealed that it binds at the base of the RBP head domain, far from the putative receptor binding site (Fig. 2A).

DISCUSSION

Recently, structural knowledge on the lactococcal phages' RBPs and their host-encoded polysaccharidic cell wall receptors has provided some insights into lactococcal phage-host interactions at an atomic level (60). The complexity of lactococcal cell wall polysaccharides explains the exquisite specificity presented by these phages for their hosts. In this context, two previous studies pertaining to the Tuc2009 baseplate made it possible to determine its overall topology and low-resolution structure (47, 48). Here, the atomic structure of the Tuc2009 tripod reveals that this host-adhesion device harbors two different carbohydrate-binding modules (CBMs), the first being a classical bona fide RBP (i.e., BppL) resembling the N-terminal domain of bc2l-c lectin from *Burkholderia cenocepacia* (52) (2WQ4), and the other, represented by the accessory protein BppA (which is absent in phage TP901-1), resembling the CBM domain of the *Thermotoga maritima* laminarinase 16a (58) (1GUI). The RBP head domain of Tuc2009 exhibits a striking flexibility, since the serendipitous head domain upper part conformation differs largely from those found in the bona fide tripod RBP or in the nano-L6/RBP complex. This flexibility may explain the difficulties encountered in the crystallization assays of Tuc2009 RBP. Noteworthy, the RBP head domain has a different fold from those of phages p2, TP901-1, and 1358, while the stem and neck share the structure of the equivalent baseplate proteins present in phage TP901-1 (Fig. 7). Nonetheless, the putative receptor binding site of Tuc2009 RBP is located in a crevice between two monomers, as is also the case for the RBPs of phages p2 and TP901-1. Analysis of the putative receptor binding sites indicates that they are very likely to be functional, in contrast to the Dit galectin domains of phages p2, TP901-1, and SPP1 in which the galectin carbohydrate-binding site is absent (23).

Indeed, phages are known to accommodate several carbohy-

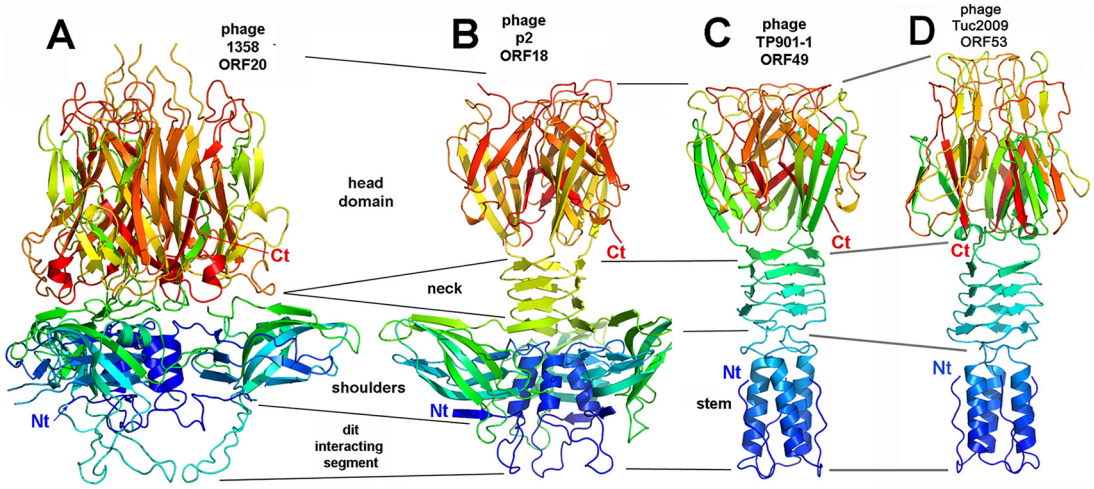

FIG 7 Comparison of the four RBPs from lactococcal phages of known structure. (A to D) RBPs of phages 1358 (40, 77) (A), p2 (53) (B), TP901-1 (25, 42) (C), and Tuc2009 (D). The RBP trimers are rainbow colored. The domains sharing structural similarities are indicated.

drate binding sites on their capsid, tail tube, and neck passage structures (60–62) for preliminary, reversible binding involved on putative host scanning. However, the final specific and irreversible binding event is exclusively linked to baseplate RBPs, as demonstrated by the use of nanobodies (23, 24) or purified RBP-containing tripods (48) as specific and effective phage competitors. The presence of two CBMs in the Tuc2009 baseplate, as opposed to the single CBM observed for TP901-1, raises questions regarding the added fitness to the phage embodied by BppA.

Other examples of multiple CBMs on phage baseplates can be deduced from their encoded protein sequences. Noteworthy, the *Lactobacillus* phages J-1 and PL-1 are predicted to possess two CBMs presented as additional domains carried by their Dit protein (63). Furthermore, the phage J1 CBM1 domain is similar to the CBM domain of the *Thermotoga maritima* laminarinase 16a (1GUI), as is BppA.

We previously reported the ability of tripods to inhibit corresponding phage from adsorbing to the host, with adsorption being the prerequisite for infection. The tripod complexes could cause nearly complete phage adsorption inhibition at a concentration as low as 1 μM. Adsorption inhibition assays were also carried out with tripods lacking BppA (48). However, the BppA-minus tripods are expected to cover the complete bacterial surface, and although its presence in the BppA-including tripod enhanced the adsorption inhibition ability at nonsaturating tripod levels, the true contribution of BppA to the adsorption process is yet to be discovered.

The structure of the receptor polysaccharide(s) at the Tuc2009 host's (*L. lactis* UC509-9) surface has not been determined yet. Our findings raise intriguing questions about Tuc2009-host interactions: does Tuc2009 recognize two different polysaccharides or two different motifs on the same polysaccharide? Indeed, these questions will only be answered upon deciphering the host's pellicle structure. Purification of this pellicle motif will make it possible to test the strength of its interaction with the CBM modules and their mode of binding, as for lactococcal phages p2 and 1358 (60).

MATERIALS AND METHODS

Protein production, purification, and crystallization. The *orf53* gene of phage Tuc2009 (encoding RBP or BppL [see the Results section]) was cloned into the Gateway destination vector pETG-20A for protein production in *E. coli* BL21, purified by Ni affinity and gel filtration chromatography according to standard procedures (64, 65).

Tuc2009 tripod preparation was published previously (48). Briefly, a DNA fragment encompassing the 3′ end of *orf51* (encoding the C-terminal portion of BppU, encompassing residues 194 to 322, and termed BppUct), *orf52* (encoding BppA), and *orf53* of phage Tuc2009 was cloned into the nisin-inducible expression vector pTX8049 for BppUctAL protein complex production in *L. lactis*. The BppUctAL protein complex was then purified by Ni affinity and gel filtration chromatography following thioredoxin removal with tobacco etch virus (TEV) protease, according to standard procedures.

With a view to obtaining nanobodies against Tuc2009 baseplate components, a dromedary camel (*Camelus dromedarius*) from the Canary Islands was immunized with Tuc2009 BppUctAL. About 300 μg of recombinant Tuc2009 tripod in phosphate-buffered saline (PBS) buffer was injected subcutaneously using Freund's adjuvant (complete the first time and incomplete for the subsequent boosters) weekly for 6 weeks, and blood samples were collected aseptically in EDTA tubes 4 days after the last booster. Lymphocytes were isolated from blood samples, and cDNA was synthesized from the acquired RNA using a reverse-PCR protocol. A nanobody phage display library of about 2×10^8 independent transformants was generated using the phagemid vector pHEN4 (66). Phage display selection and screening of specific nanobodies were performed as previously published (45). A clear enrichment of antigen-specific clones was observed after three consecutive rounds of selection on solid-phase-coated antigen. After the third round, nano-L06, specific for BppL, was identified, after which the insert of the corresponding pHEN4-derived plasmid was sequenced and the relevant sequence cloned into the pHEN6 vector (67). Nanobody (nano-L06) expression and purification were performed as previously described (67).

The nano-L06 nanobody was subjected to crystallization screening with a TTP Labtech Mosquito device in Greiner Bio-One CrystalQuick plates. Crystals were obtained at 20°C by mixing 100 to 300 nl of 12 mg·ml^{-1} protein (Na_2HPO_4, 10 mM; KH_2PO_4, 1.8 mM [pH 7.4]; NaCl, 137 mM; KCl, 2.7 mM) with 100 nl precipitant solution in 25 to 30% polyethylene glycol (PEG) 4000–0.2 M imidazole (pH 6.0). BppL and nano-L06 were mixed at a ratio of 1:2 (mol/mol). The complex was subjected to trypsin digestion (1,000:1 mol/mol) at room temperature for 2 h and immediately purified on Superdex 200 26/600 (GE Healthcare) in PBS at pH 7.4. It was then concentrated to 9 mg·ml^{-1} with a 30-kDa-cutoff Amicon-Ultra for crystallization assays with a TTP Labtech Mosquito in Greiner Bio-One CrystalQuick plates. Crystals were obtained at 20°C by mixing 300 nl of protein (10 mM HEPES [pH 7.5], 150 mM NaCl) with 100 nl precipitant solution (25 to 30% PEG 4000, 0.2 M imidazole [pH 6.0], or 0.1 M Tris [pH 8.0]).

The tripod complex of 280 kDa, as determined by size exclusion chromatography-UV multiangle light scattering (SEC-UV-MALS) (48), was concentrated to 10 mg/ml and subjected to crystallization screening with a TTP Labtech Mosquito in Greiner Bio-One CrystalQuick plates. Crystals were obtained at 20°C by mixing 300 nl of protein (Na_2HPO_4, 10 mM; KH_2PO_4, 1.8 mM [pH 7.4]; NaCl, 137 mM; KCl, 2.7 mM) with 100 nl precipitant solution (2 M ammonium sulfate, 0.1 M Na HEPES [pH 7]).

Crystal structure determination. Crystals of the nano-L06 nanobody were cryocooled without cryo-protectant, and data sets were collected at Soleil Proxima 1 (Soleil synchrotron, Saint-Aubin, France) at wavelengths of 1.7712 Å (1.90-Å resolution) and 0.86 Å (1.1-Å resolution). Data were treated with XDS and XSCALE (68). The nano-L06 crystal was shown to belong to space group $P6_522$ with cell dimensions $a = b = 52.1$ Å and $c = 162.7$ Å and to contain 44.6% solvent for a molecule per asymmetric unit. The structure was determined by sulfur single-wavelength anomalous dispersion (S-SAD) with the data set collected at the wavelength of 1.7712 Å. Five initial sulfur sites (three individual methionines plus two cysteines involved in a disulfide bond) were located with the SHELXC/D programs (69). Using the program Phaser (70), the heavy-atom model was then completed up to 7 sulfur sites, and phases were refined before being improved by density modification using Parrot (71). The first steps of model building were performed automatically using Buccaneer (72) and completed manually with Coot (73). The model was finally refined using the high-resolution data set collected at a 1.1-Å resolution with refmac and Phenix (74, 75).

A crystal of the complex nano-L06/RBP was cryocooled in trimethylamine *N*-oxide (TMAO) or 10% PEG 600, and a data set was collected at Soleil Proxima 1 (Soleil synchrotron, Saint-Aubin, France) up to a 2.70-Å resolution. It was demonstrated to belong to space group $P2_12_12_1$ with cell dimensions $a = 84.7$ Å, $b = 88.04$ Å, and $c = 147.6$ Å. Molecular replacement was performed with Molrep using the refined structure of nano-L06. It yielded three nano-L06 molecules related by a 3-fold axis and good statistics and packing. Initial refinement was performed with AutoBUSTER (76) using dummy water molecules to complete the model, allowing further positioning of several β-strands. After density modification using Parrot (71), the model was further automatically refined using Buccaneer (72) and then completed manually with Coot (73). The resulting final structure, however, consisted only of the trimeric head domain

and an N-terminal β-helix, indicating that the stem had been removed during trypsin cleavage.

A crystal of the Tuc2009 tripod BppUctAL complex was cryocooled in TMAO, and a data set was collected at Soleil Proxima 1 (Soleil synchrotron, Saint-Aubin, France) up to a 2.9-Å resolution. It was shown to belong to the cubic space group $P2_13$ with cell dimensions $a = b = c =$ 212.0 Å. Molecular replacement was performed with Phaser (70) using an ensemble1 comprising BppUct and the N-terminal part of the BppL trimer (3 × residues 2 to 30) and as ensemble2 a monomer of the BppL head structure as determined above, yet depleted of its N-terminal helix. Phaser yielded a solution comprising a unique ensemble1, but forming a trimer reconstituted by the cubic 3-fold axis, and a trimer of ensemble2 representing the BppL/RBP head trimer. Initial refinement was performed with AutoBUSTER (76) using dummy water molecules to complete the model, allowing further positioning of several β-strands between the BppL N terminus and head, where the expected BppL β-helix should be found, and at other positions that we presumed to be part of BppA. After density modification using Parrot (71), the model was further automatically refined using Buccaneer (72) and then manually completed with Coot (73), thereby yielding the BppL stem domain and the complete BppA. At this stage, some extra density was still visible. After manual construction with Coot (73), we could identify the presence of a BppL head domain sitting on the cubic 3-fold axis that reconstituted a BppL head trimer.

Modeling of the phage Tuc2009 baseplate. The BppU C-terminal domain of the TP901-1 baseplate, being highly similar to that of Tuc2009, was used as a template to fit the Tuc2009 tripod onto the TP901-1 BppU/Dit complex. Using Coot (73) option "SSM superpose," we used the Tuc2009 BppUct domain of each tripod as the "source" structure and the BppUct domain of TP901-1 baseplate as the "target." Following this, the TP901-1 baseplate BppL and BppUct components were deleted. Furthermore, the most internal BppA modules of each Tuc2009 tripod had to be removed from the tripod as they physically clash with full-length BppU (48).

BLI. Prior to biolayer interferometry (BLI) assays, nano-L06 was biotinylated at a 1:1 ratio using the EZ-Link NHS-PEG4-biotin kit (Perbio Science, France). The reaction was stopped by removing the excess of biotin reagent using a Zeba Spin desalting column (Perbio Science, France). OctetRed96 (ForteBio, United States) was used for BLI studies. Assays were performed in black 96-well plates. The total working volume for samples or buffer was 0.2 ml, and the revolutions-per-minute setting was 1,000 rpm for baseline, loading, association, and dissociation steps. The experiments were performed at 25°C. Prior to each assay, streptavidin (SA) biosensor tips (ForteBio, USA) were hydrated in 0.2 ml kinetic buffer (KB; ForteBio, USA) for 20 min. The SA biosensor tips were then loaded with biotinylated nano-L06 at 5 μg/ml in KB, followed by a quenching step using biocytin. A baseline was recorded, and nano-L06 binding to RBP was monitored at concentrations of 0.22 to 140 nM. Association and dissociation were carried out for 400 s and 600 s, respectively. Complete dissociation of the complex was achieved by 3-fold regeneration (5 s in glycine 10 mM [pH 1.7]) and neutralization (5 s in KB). For the tripod, the same protocol was applied with a concentration range of 0.24 to 530 nM.

Neutralization studies. Neutralization assays were performed as described previously (45). Briefly, bromocresol purple (BCP) broth (3 ml) supplemented with 10 mM calcium chloride was the background medium in which the neutralization assays were performed. Nanobody nano-L06 was assessed for neutralization of infection by preincubating 10^5 PFU Tuc2009 and nanobody at 0.05, 0.1, 1, 2, 5, 20, and 50 μg/ml for 1 h at 30°C before addition of 45 μl of a fresh overnight culture of the host, *L. lactis* UC509.9 (10^7 CFU), and further incubation for 7 h at 30°C. Controls were included to validate the assay, whereby the host alone (*L. lactis* UC509.9) or the host and its infecting phage (*L. lactis* UC509.9 plus Tuc2009) were applied to show growth or lack of growth due to phage infection, respectively. Color change from purple to yellow indicated acidification and therefore growth of *L. lactis* UC509.9, whereas a purple color indicated lack of growth and thus phage infection.

SUPPLEMENTAL MATERIAL

Supplemental material for this article may be found at http://mbio.asm.org/lookup/suppl/doi:10.1128/mBio.01781-15/-/DCSupplemental.

Table S1, DOCX file, 0.2 MB.

ACKNOWLEDGMENTS

We thank the Soleil synchrotron (France) for the beam time allocation (proposal 20140754).

This work was supported by grants from the Agence Nationale de la Recherche (grants ANR-11-BSV8-004-01 "Lactophages" and French Infrastructure for Integrated Structural Biology [FRISBI]). D. van Sinderen is supported by a Principal Investigator award (reference no. 13/IA/1953) through Science Foundation Ireland (SFI). J. Mahony is the recipient of a Technology Innovation Development Award (TIDA) (reference no. 14/TIDA/2287) funded by Science Foundation Ireland (SFI).

FUNDING INFORMATION

Science Foundation Ireland (SFI) provided funding to Douwe van Sinderen under grant number 13/IA/1953. Science Foundation Ireland (SFI) provided funding to Jennifer Mahony under grant number 14/TIDA/2287. Agence Nationale de la Recherche (ANR) provided funding to Christian Cambillau under grant number ANR-11-BSV8-004-01. French Infrastructure for Integrated Structural Biology (FRISBI) provided funding to C. Cambillau under grant number ANR-10-INSB-05-01.

REFERENCES

1. **Davidson AR, Cardarelli L, Pell LG, Radford DR, Maxwell KL.** 2012. Long noncontractile tail machines of bacteriophages. Adv Exp Med Biol **726:**115–142. http://dx.doi.org/10.1007/978-1-4614-0980-9_6.
2. **Effantin G, Boulanger P, Neumann E, Letellier L, Conway JF.** 2006. Bacteriophage T5 structure reveals similarities with HK97 and T4 suggesting evolutionary relationships. J Mol Biol **361:**993–1002. http://dx.doi.org/10.1016/j.jmb.2006.06.081.
3. **Fokine A, Chipman PR, Leiman PG, Mesyanzhinov VV, Rao VB, Rossmann MG.** 2004. Molecular architecture of the prolate head of bacteriophage T4. Proc Natl Acad Sci U S A **101:**6003–6008. http://dx.doi.org/10.1073/pnas.0400444101.
4. **Morais MC, Choi KH, Koti JS, Chipman PR, Anderson DL, Rossmann MG.** 2005. Conservation of the capsid structure in tailed dsDNA bacteriophages: the pseudoatomic structure of phi29. Mol Cell **18:** 149–159. http://dx.doi.org/10.1016/j.molcel.2005.03.013.
5. **Pell LG, Gasmi-Seabrook GM, Morais M, Neudecker P, Kanelis V, Bona D, Donaldson LW, Edwards AM, Howell PL, Davidson AR, Maxwell KL.** 2010. The solution structure of the C-terminal Ig-like domain of the bacteriophage lambda tail tube protein. J Mol Biol **403:**468–479. http://dx.doi.org/10.1016/j.jmb.2010.08.044.
6. **Plisson C, White HE, Auzat I, Zafarani A, São-José C, Lhuillier S, Tavares P, Orlova EV.** 2007. Structure of bacteriophage SPP1 tail reveals trigger for DNA ejection. EMBO J **26:**3720–3728. http://dx.doi.org/10.1038/sj.emboj.7601786.
7. **Parent KN, Erb ML, Cardone G, Nguyen K, Gilcrease EB, Porcek NB, Pogliano J, Baker TS, Casjens SR.** 2014. OmpA and OmpC are critical host factors for bacteriophage Sf6 entry in Shigella. Mol Microbiol **92:** 47–60. http://dx.doi.org/10.1111/mmi.12536.
8. **Hu B, Margolin W, Molineux IJ, Liu J.** 2013. The bacteriophage T7 virion undergoes extensive structural remodeling during infection. Science **339:**576–579. http://dx.doi.org/10.1126/science.1231887.
9. **Kostyuchenko VA, Leiman PG, Chipman PR, Kanamaru S, van Raaij MJ, Arisaka F, Mesyanzhinov VV, Rossmann MG.** 2003. Three-dimensional structure of bacteriophage T4 baseplate. Nat Struct Biol **10:** 688–693. http://dx.doi.org/10.1038/nsb970.
10. **Mahony J, van Sinderen D.** 2015. Gram-positive phage-host interactions. Front Microbiol **6:**61. http://dx.doi.org/10.3389/fmicb.2015.00061.
11. **Aksyuk AA, Leiman PG, Kurochkina LP, Shneider MM, Kostyuchenko VA, Mesyanzhinov VV, Rossmann MG.** 2009. The tail sheath structure of

bacteriophage T4: a molecular machine for infecting bacteria. EMBO J **28:**821–829. http://dx.doi.org/10.1038/emboj.2009.36.
12. **Kanamaru S, Leiman PG, Kostyuchenko VA, Chipman PR, Mesyanzhinov VV, Arisaka F, Rossmann MG.** 2002. Structure of the cell-puncturing device of bacteriophage T4. Nature **415:**553–557. http://dx.doi.org/10.1038/415553a.
13. **Leiman PG, Battisti AJ, Bowman VD, Stummeyer K, Mühlenhoff M, Gerardy-Schahn R, Scholl D, Molineux IJ.** 2007. The structures of bacteriophages K1E and K1-5 explain processive degradation of polysaccharide capsules and evolution of new host specificities. J Mol Biol **371:**836–849. http://dx.doi.org/10.1016/j.jmb.2007.05.083.
14. **Valyasevi R, Sandine WE, Geller BL.** 1991. A membrane protein is required for bacteriophage c2 infection of Lactococcus lactis subsp. lactis C2. J Bacteriol **173:**6095–6100.
15. **Dupont K, Janzen T, Vogensen FK, Josephsen J, Stuer-Lauridsen B.** 2004. Identification of Lactococcus lactis genes required for bacteriophage adsorption. Appl Environ Microbiol **70:**5825–5832. http://dx.doi.org/10.1128/AEM.70.10.5825-5832.2004.
16. **Randall-Hazelbauer L, Schwartz M.** 1973. Isolation of the bacteriophage lambda receptor from Escherichia coli. J Bacteriol **116:**1436–1446.
17. **Wang J, Michel V, Hofnung M, Charbit A.** 1998. Cloning of the J gene of bacteriophage lambda, expression and solubilization of the J protein: first in vitro studies on the interactions between J and LamB, its cell surface receptor. Res Microbiol **149:**611–624. http://dx.doi.org/10.1016/S0923-2508(99)80009-6.
18. **Bonhivers M, Letellier L.** 1995. Calcium controls phage T5 infection at the level of the Escherichia coli cytoplasmic membrane. FEBS Lett **374:**169–173. http://dx.doi.org/10.1016/0014-5793(95)01101-J.
19. **Plançon L, Janmot C, le Maire M, Desmadril M, Bonhivers M, Letellier L, Boulanger P.** 2002. Characterization of a high-affinity complex between the bacterial outer membrane protein FhuA and the phage T5 protein pb5. J Mol Biol **318:**557–569. http://dx.doi.org/10.1016/S0022-2836(02)00089-X.
20. **Baptista C, Santos MA, São-José C.** 2008. Phage SPP1 reversible adsorption to Bacillus subtilis cell wall teichoic acids accelerates virus recognition of membrane receptor YueB. J Bacteriol **190:**4989–4996. http://dx.doi.org/10.1128/JB.00349-08.
21. **São-José C, Lhuillier S, Lurz R, Melki R, Lepault J, Santos MA, Tavares P.** 2006. The ectodomain of the viral receptor YueB forms a fiber that triggers ejection of bacteriophage SPP1 DNA. J Biol Chem **281:**11464–11470. http://dx.doi.org/10.1074/jbc.M513625200.
22. **Bebeacua C, Bron P, Lai L, Vegge CS, Brøndsted L, Spinelli S, Campanacci V, Veesler D, van Heel M, Cambillau C.** 2010. Structure and molecular assignment of lactococcal phage TP901-1 baseplate. J Biol Chem **285:**39079–39086. http://dx.doi.org/10.1074/jbc.M110.175646.
23. **Sciara G, Bebeacua C, Bron P, Tremblay D, Ortiz-Lombardia M, Lichière J, van Heel M, Campanacci V, Moineau S, Cambillau C.** 2010. Structure of lactococcal phage p2 baseplate and its mechanism of activation. Proc Natl Acad Sci U S A **107:**6852–6857. http://dx.doi.org/10.1073/pnas.1000232107.
24. **Veesler D, Dreier B, Blangy S, Lichière J, Tremblay D, Moineau S, Spinelli S, Tegoni M, Plückthun A, Campanacci V, Cambillau C.** 2009. Crystal structure and function of a DARPin neutralizing inhibitor of lactococcal phage TP901-1: comparison of DARPin and camelid VHH binding mode. J Biol Chem **284:**30718–30726. http://dx.doi.org/10.1074/jbc.M109.037812.
25. **Veesler D, Spinelli S, Mahony J, Lichière J, Blangy S, Bricogne G, Legrand P, Ortiz-Lombardia M, Campanacci V, van Sinderen D, Cambillau C.** 2012. Structure of the phage TP901-1 1.8 MDa baseplate suggests an alternative host adhesion mechanism. Proc Natl Acad Sci U S A **109:**8954–8958. http://dx.doi.org/10.1073/pnas.1200966109.
26. **Yu F, Mizushima S.** 1982. Roles of lipopolysaccharide and outer membrane protein OmpC of Escherichia coli K-12 in the receptor function for bacteriophage T4. J Bacteriol **151:**718–722.
27. **Bartual SG, Otero JM, Garcia-Doval C, Llamas-Saiz AL, Kahn R, Fox GC, van Raaij MJ.** 2010. Structure of the bacteriophage T4 long tail fiber receptor-binding tip. Proc Natl Acad Sci U S A **107:**20287–20292. http://dx.doi.org/10.1073/pnas.1011218107.
28. **Rossmann MG, Mesyanzhinov VV, Arisaka F, Leiman PG.** 2004. The bacteriophage T4 DNA injection machine. Curr Opin Struct Biol **14:**171–180. http://dx.doi.org/10.1016/j.sbi.2004.02.001.
29. **Leiman PG, Arisaka F, van Raaij MJ, Kostyuchenko VA, Aksyuk AA, Kanamaru S, Rossmann MG.** 2010. Morphogenesis of the T4 tail and tail fibers. Virol J **7:**355. http://dx.doi.org/10.1186/1743-422X-7-355.
30. **Riede I.** 1987. Receptor specificity of the short tail fibres (gp12) of T-even type Escherichia coli phages. Mol Gen Genet **206:**110–115. http://dx.doi.org/10.1007/BF00326544.
31. **Murphy J, Royer B, Mahony J, Hoyles L, Heller K, Neve H, Bonestroo M, Nauta A, van Sinderen D.** 2013. Biodiversity of lactococcal bacteriophages isolated from 3 Gouda-type cheese-producing plants. J Dairy Sci **96:**4945–4957. http://dx.doi.org/10.3168/jds.2013-6748.
32. **Szczepańska AK, Hejnowicz MS, Kołakowski P, Bardowski J.** 2007. Biodiversity of Lactococcus lactis bacteriophages in Polish dairy environment. Acta Biochim Pol **54:**151–158.
33. **Deveau H, Labrie SJ, Chopin MC, Moineau S.** 2006. Biodiversity and classification of lactococcal phages. Appl Environ Microbiol **72:**4338–4346. http://dx.doi.org/10.1128/AEM.02517-05.
34. **Kleppen HP, Bang T, Nes IF, Holo H.** 2011. Bacteriophages in milk fermentations: diversity fluctuations of normal and failed fermentations. Int Dairy J **21:**592–600. http://dx.doi.org/10.1016/j.idairyj.2011.02.010.
35. **Castro-Nallar E, Chen H, Gladman S, Moore SC, Seemann T, Powell IB, Hillier A, Crandall KA, Chandry PS.** 2012. Population genomics and phylogeography of an Australian dairy factory derived lytic bacteriophage. Genome Biol Evol **4:**382–393. http://dx.doi.org/10.1093/gbe/evs017.
36. **Moineau S, Borkaev M, Holler BJ, Walker SA, Kondo JK, Vedamuthu ER, Vandenbergh PA.** 1996. Isolation and characterization of lactococcal bacteriophages from cultured buttermilk plants in the United States. J Dairy Sci **79:**2104–2111. http://dx.doi.org/10.3168/jds.S0022-0302(96)76584-0.
37. **Rousseau GM, Moineau S.** 2009. Evolution of Lactococcus lactis phages within a cheese factory. Appl Environ Microbiol **75:**5336–5344. http://dx.doi.org/10.1128/AEM.00761-09.
38. **Chapot-Chartier MP, Vinogradov E, Sadovskaya I, Andre G, Mistou MY, Trieu-Cuot P, Furlan S, Bidnenko E, Courtin P, Péchoux C, Hols P, Dufrêne YF, Kulakauskas S.** 2010. Cell surface of Lactococcus lactis is covered by a protective polysaccharide pellicle. J Biol Chem **285:**10464–10471. http://dx.doi.org/10.1074/jbc.M109.082958.
39. **Ainsworth S, Sadovskaya I, Vinogradov E, Courtin P, Guerardel Y, Mahony J, Grard T, Cambillau C, Chapot-Chartier MP, van Sinderen D.** 2014. Differences in lactococcal cell wall polysaccharide structure are major determining factors in bacteriophage sensitivity. mBio **5:**e00880-14. http://dx.doi.org/10.1128/mBio.00880-14.
40. **Farenc C, Spinelli S, Vinogradov E, Tremblay D, Blangy S, Sadovskaya I, Moineau S, Cambillau C.** 2014. Molecular insights on the recognition of a Lactococcus lactis cell wall pellicle by the phage 1358 receptor binding protein. J Virol **88:**7005–7015. http://dx.doi.org/10.1128/JVI.00739-14.
41. **Ricagno S, Campanacci V, Blangy S, Spinelli S, Tremblay D, Moineau S, Tegoni M, Cambillau C.** 2006. Crystal structure of the receptor-binding protein head domain from Lactococcus lactis phage bIL170. J Virol **80:**9331–9335. http://dx.doi.org/10.1128/JVI.01160-06.
42. **Spinelli S, Campanacci V, Blangy S, Moineau S, Tegoni M, Cambillau C.** 2006. Modular structure of the receptor binding proteins of Lactococcus lactis phages. The RBP structure of the temperate phage TP901-1. J Biol Chem **281:**14256–14262. http://dx.doi.org/10.1074/jbc.M600666200.
43. **Shepherd DA, Veesler D, Lichière J, Ashcroft AE, Cambillau C.** 2011. Unraveling lactococcal phage baseplate assembly by mass spectrometry. Mol Cell Proteomics **10:**M111.009787. http://dx.doi.org/10.1074/mcp.M111.009787.
44. **Mahony J, Tremblay DM, Labrie SJ, Moineau S, van Sinderen D.** 2015. Investigating the requirement for calcium during lactococcal phage infection. Int J Food Microbiol **201:**47–51. http://dx.doi.org/10.1016/j.ijfoodmicro.2015.02.017.
45. **Desmyter A, Farenc C, Mahony J, Spinelli S, Bebeacua C, Blangy S, Veesler D, van Sinderen D, Cambillau C.** 2013. Viral infection modulation and neutralization by camelid nanobodies. Proc Natl Acad Sci U S A **110:**E1371–E1379. http://dx.doi.org/10.1073/pnas.1301336110.
46. **Ainsworth S, Zomer A, de Jager V, Bottacini F, van Hijum SA, Mahony J, van Sinderen D.** 2013. Complete genome of Lactococcus lactis subsp. cremoris UC509.9, host for a model lactococcal P335 bacteriophage. Genome Announc **1:**e00119-12. http://dx.doi.org/10.1128/genomeA.00119-12.
47. **Sciara G, Blangy S, Siponen M, McGrath S, van Sinderen D, Tegoni M, Cambillau C, Campanacci V.** 2008. A topological model of the baseplate

of lactococcal phage Tuc2009. J Biol Chem **283:**2716–2723. http://dx.doi.org/10.1074/jbc.M707533200.
48. **Collins B, Bebeacua C, Mahony J, Blangy S, Douillard FP, Veesler D, Cambillau C, van Sinderen D.** 2013. Structure and functional analysis of the host recognition device of lactococcal phage Tuc2009. J Virol **87:**8429–8440. http://dx.doi.org/10.1128/JVI.00907-13.
49. **Desmyter A, Spinelli S, Roussel A, Cambillau C.** 2015. Camelid nanobodies: killing two birds with one stone. Curr Opin Struct Biol **32:**1–8. http://dx.doi.org/10.1016/j.sbi.2015.01.001.
50. **Krissinel E, Henrick K.** 2007. Inference of macromolecular assemblies from crystalline state. J Mol Biol **372:**774–797. http://dx.doi.org/10.1016/j.jmb.2007.05.022.
51. **Holm L, Kääriäinen S, Rosenström P, Schenkel A.** 2008. Searching protein structure databases with DaliLite v.3. Bioinformatics **24:**2780–2781. http://dx.doi.org/10.1093/bioinformatics/btn507.
52. **Sulák O, Cioci G, Delia M, Lahmann M, Varrot A, Imberty A, Wimmerová M.** 2010. A TNF-like trimeric lectin domain from Burkholderia cenocepacia with specificity for fucosylated human histo-blood group antigens. Structure **18:**59–72. http://dx.doi.org/10.1016/j.str.2009.10.021.
53. **Spinelli S, Desmyter A, Verrips CT, de Haard HJ, Moineau S, Cambillau C.** 2006. Lactococcal bacteriophage p2 receptor-binding protein structure suggests a common ancestor gene with bacterial and mammalian viruses. Nat Struct Mol Biol **13:**85–89. http://dx.doi.org/10.1038/nsmb1029.
54. **Campanacci V, Veesler D, Lichière J, Blangy S, Sciara G, Moineau S, van Sinderen D, Bron P, Cambillau C.** 2010. Solution and electron microscopy characterization of lactococcal phage baseplates expressed in Escherichia coli. J Struct Biol **172:**75–84. http://dx.doi.org/10.1016/j.jsb.2010.02.007.
55. **Vagin A, Teplyakov A.** 2010. Molecular replacement with MOLREP. Acta Crystallogr D Biol Crystallogr **66:**22–25. http://dx.doi.org/10.1107/S0907444909042589.
56. **McCoy AJ.** 2007. Solving structures of protein complexes by molecular replacement with Phaser. Acta Crystallogr D Biol Crystallogr **63:**32–41. http://dx.doi.org/10.1107/S0907444906045975.
57. **Pettersen EF, Goddard TD, Huang CC, Couch GS, Greenblatt DM, Meng EC, Ferrin TE.** 2004. UCSF Chimera—a visualization system for exploratory research and analysis. J Comput Chem **25:**1605–1612. http://dx.doi.org/10.1002/jcc.20084.
58. **Boraston AB, Nurizzo D, Notenboom V, Ducros V, Rose DR, Kilburn DG, Davies GJ.** 2002. Differential oligosaccharide recognition by evolutionarily-related beta-1,4 and beta-1,3 glucan-binding modules. J Mol Biol **319:**1143–1156. http://dx.doi.org/10.1016/S0022-2836(02)00374-1.
59. **Mrosek M, Labeit D, Witt S, Heerklotz H, von Castelmur E, Labeit S, Mayans O.** 2007. Molecular determinants for the recruitment of the ubiquitin-ligase MuRF-1 onto M-line titin. FASEB J **21:**1383–1392. http://dx.doi.org/10.1096/fj.06-7644com.
60. **Spinelli S, Veesler D, Bebeacua C, Cambillau C.** 2014. Structures and host-adhesion mechanisms of lactococcal siphophages. Front Microbiol **5:**3. http://dx.doi.org/10.3389/fmicb.2014.00003.
61. **Bebeacua C, Tremblay D, Farenc C, Chapot-Chartier MP, Sadovskaya I, van Heel M, Veesler D, Moineau S, Cambillau C.** 2013. Structure, adsorption to host, and infection mechanism of virulent lactococcal phage p2. J Virol **87:**12302–12312. http://dx.doi.org/10.1128/JVI.02033-13.
62. **Xiang Y, Rossmann MG.** 2011. Structure of bacteriophage phi29 head fibers has a supercoiled triple repeating helix-turn-helix motif. Proc Natl Acad Sci U S A **108:**4806–4810. http://dx.doi.org/10.1073/pnas.1018097108.
63. **Dieterle ME, Bowman C, Batthyany C, Lanzarotti E, Turjanski A, Hatfull G, Piuri M.** 2014. Exposing the secrets of two well-known Lactobacillus casei phages, J-1 and PL-1, by genomic and structural analysis. Appl Environ Microbiol **80:**7107–7121. http://dx.doi.org/10.1128/AEM.02771-14.
64. **Vincentelli R, Canaan S, Offant J, Cambillau C, Bignon C.** 2005. Automated expression and solubility screening of His-tagged proteins in 96-well format. Anal Biochem **346:**77–84. http://dx.doi.org/10.1016/j.ab.2005.07.039.
65. **Vincentelli R, Bignon C, Gruez A, Canaan S, Sulzenbacher G, Tegoni M, Campanacci V, Cambillau C.** 2003. Medium-scale structural genomics: strategies for protein expression and crystallization. Acc Chem Res **36:**165–172. http://dx.doi.org/10.1021/ar010130s.
66. **Pardon E, Laeremans T, Triest S, Rasmussen SG, Wohlkönig A, Ruf A, Muyldermans S, Hol WG, Kobilka BK, Steyaert J.** 2014. A general protocol for the generation of nanobodies for structural biology. Nat Protoc **9:**674–693. http://dx.doi.org/10.1038/nprot.2014.039.
67. **Conrath K, Pereira AS, Martins CE, Timóteo CG, Tavares P, Spinelli S, Kinne J, Flaudrops C, Cambillau C, Muyldermans S, Moura I, Moura JJ, Tegoni M, Desmyter A.** 2009. Camelid nanobodies raised against an integral membrane enzyme, nitric oxide reductase. Protein Sci **18:**619–628. http://dx.doi.org/10.1002/pro.69.
68. **Kabsch W.** 2010. XDS. Acta Crystallogr D Biol Crystallogr **66:**125–132. http://dx.doi.org/10.1107/S0907444909047337.
69. **Schneider TR, Sheldrick GM.** 2002. Substructure solution with SHELXD. Acta Crystallogr D Biol Crystallogr **58:**1772–1779. http://dx.doi.org/10.1107/S0907444902011678.
70. **McCoy AJ, Grosse-Kunstleve RW, Adams PD, Winn MD, Storoni LC, Read RJ.** 2007. Phaser crystallographic software. J Appl Crystallogr **40:**658–674. http://dx.doi.org/10.1107/S0021889807021206.
71. **Cowtan K.** 2010. Recent developments in classical density modification. Acta Crystallogr D Biol Crystallogr **66:**470–478. http://dx.doi.org/10.1107/S090744490903947X.
72. **Cowtan K.** 2006. The buccaneer software for automated model building. 1. Tracing protein chains. Acta Crystallogr D Biol Crystallogr **62:**1002–1011. http://dx.doi.org/10.1107/S0907444906022116.
73. **Emsley P, Lohkamp B, Scott WG, Cowtan K.** 2010. Features and development of coot. Acta Crystallogr D Biol Crystallogr **66:**486–501. http://dx.doi.org/10.1107/S0907444910007493.
74. **Adams PD, Afonine PV, Bunkóczi G, Chen VB, Davis IW, Echols N, Headd JJ, Hung LW, Kapral GJ, Grosse-Kunstleve RW, McCoy AJ, Moriarty NW, Oeffner R, Read RJ, Richardson DC, Richardson JS, Terwilliger TC, Zwart PH.** 2010. PHENIX: a comprehensive python-based system for macromolecular structure solution. Acta Crystallogr D Biol Crystallogr **66:**213–221. http://dx.doi.org/10.1107/S0907444909052925.
75. **Murshudov GN, Skubák P, Lebedev AA, Pannu NS, Steiner RA, Nicholls RA, Winn MD, Long F, Vagin AA.** 2011. REFMAC5 for the refinement of macromolecular crystal structures. Acta Crystallogr D Biol Crystallogr **67:**355–367. http://dx.doi.org/10.1107/S0907444911001314.
76. **Blanc E, Roversi P, Vonrhein C, Flensburg C, Lea SM, Bricogne G.** 2004. Refinement of severely incomplete structures with maximum likelihood in BUSTER-TNT. Acta Crystallogr D Biol Crystallogr **60:**2210–2221. http://dx.doi.org/10.1107/S0907444904016427.
77. **McCabe O, Spinelli S, Farenc C, Labbé M, Tremblay D, Blangy S, Oscarson S, Moineau S, Cambillau C.** 2015. The targeted recognition of Lactococcus lactis phages to their polysaccharide receptors. Mol Microbiol **96:**875–886 http://dx.doi.org/10.1111/mmi.12978.